Nitrogen Oxide Emissions from U.S. Oil and Gas Production: Recent Trends and Source Attribution

Barbara Dix[1], Joep de Bruin[1,2*], Esther Roosenbrand[1,2], Tim Vlemmix[3], Colby Francoeur[1,4], Alan Gorchov-Negron[5], Brian McDonald[1,4], Mikhail Zhizhin[1,6,7], Christopher Elvidge[7], Pepijn Veefkind[2,3], Pieternel Levelt[2,3], Joost de Gouw[1,8]

[1]Cooperative Institute for Research in Environmental Sciences, University of Colorado Boulder, Boulder, CO, USA.

[2]Department of Geoscience and Remote Sensing, Civil Engineering and Geosciences, Technical University of Delft, the Netherlands.

[3]Royal Netherlands Meteorological Institute, De Bilt, the Netherlands.

[4]NOAA Earth System Research Laboratory, Chemical Sciences Division, Boulder, CO, USA.

[5]Department of Climate and Space Sciences and Engineering, University of Michigan, Ann Arbor, MI, USA.

[6]NOAA National Centers for Environmental Information, Earth Observation Group, Boulder, CO, USA.

[7]The Payne Institute for Public Policy, Colorado School of Mines, Golden, CO, USA.

[8]Department of Chemistry, University of Colorado Boulder, Boulder, CO, USA.

[*]now at Concentra Analytics, the Hague, the Netherlands.

Corresponding author: Barbara Dix (Barbara.Dix@colorado.edu), Joost de Gouw (Joost.deGouw@colorado.edu)

Key Points:

- Recent increases in U.S. oil and gas production are seen from space as increased tropospheric NO_2 columns and increased gas flaring.
- Changes in NO_2 over time can be attributed to oil and gas NO_x emissions associated with drilling, production and gas flaring activities.
- Top-down and bottom-up source attributions agree that drilling and, to a lesser extent, production are the main sources of NO_x emissions.

This is the author manuscript accepted for publication and has undergone full peer review but has not been through the copyediting, typesetting, pagination and proofreading process, which may lead to differences between this version and the Version of Record. Please cite this article as doi: 10.1029/2019GL085866

Abstract

U.S. oil and natural gas production volumes have grown by up to 100% in key production areas between January 2017 and August 2019. Here we show that recent trends are visible from space and can be attributed to drilling, production and gas flaring activities. By using oil and gas activity data as predictors in a multivariate regression to satellite measurements of tropospheric NO_2 columns, observed changes in NO_2 over time could be attributed to NO_x emissions associated with drilling, production and gas flaring for three select regions: the Permian, Bakken and Eagle Ford basins. We find that drilling had been the dominant NO_x source contributing around 80% before the downturn in drilling activity in 2015. Thereafter, NO_x contributions from drilling activities and combined production and flaring activities are similar. Comparison of our top-down source attribution with a bottom-up fuel-based oil and gas NO_x emission inventory shows agreement within error margins.

Plain Language Summary

U.S. oil and natural gas production volumes have grown by up to 100% in key production areas between January 2017 and August 2019. Here we show that recent trends are visible from space as increases in NO_2, an air pollutant that is released from combustion engines associated with the oil and gas industry. For three select regions, the Permian (TX and NM), Bakken (ND) and Eagle Ford (TX) basins, we report that the trend in NO_2 columns over time can be explained by a combination of drilling activity, production numbers and flared gas volume, which allows us to quantify the contributions from these sources to the total NO_x (= NO + NO_2) emissions from these areas. We find that drilling had been the dominant NO_x source contributing around 80% before the downturn in drilling activity in 2015. But now, NO_x contributions from drilling activities and combined production and flaring activities are similar. Both Permian and Bakken oil and gas production volumes are at an all-time high and if current growth rates continue in the Eagle Ford basin, maximum production volumes will be exceeded in about one year.

1 Introduction

Since the mid-2000s the development and widespread use of horizontal drilling and hydraulic fracturing has led to rapid increases in the production of oil and natural gas in the United States. The abundant supply of natural gas has facilitated the ongoing replacement of coal as a fuel for electric power production, with important benefits to emissions of carbon dioxide and air pollutants such as nitrogen oxides (NO_x=NO+NO_2), and sulfur dioxide (de Gouw et al., 2014). In contrast, leaks of methane, the major component of natural gas, from exploration and production offset the advantages of natural gas for total greenhouse gas emissions (Alvarez et al., 2012; 2018; Brandt et al., 2014; Karion et al., 2013). The production of oil and natural gas is also associated with emissions of NO_x, and other air pollutants like volatile organic compounds and air toxics (benzene, hydrogen sulfide) (Petron et al., 2012; Warneke et al., 2014). NO_x is directly associated with impacting the respiratory system (WHO 2005) and plays a key role in the photochemical production of tropospheric ozone and other secondary pollutants. Elevated ozone

has been observed in oil and gas production regions and attributed to these emissions (Edwards et al., 2014). The quantification and reduction of these air pollutant and greenhouse gas emissions from oil and gas production are essential to mitigate the effects on air quality, human health and climate change.

Emissions can be quantified bottom-up, using documented oil and gas activity and emission factor data, or top-down, where emissions are derived using atmospheric measurements. Studies have demonstrated significant discrepancies between these two methods, implying that oil and gas emission sources are not fully understood (Ahmadov et al., 2015; Alvarez et al., 2018; Gorchov Negron et al., 2018). NO_x and methane emissions over oil and gas production areas have been observed from space. Satellite data are important, because surface measurements are limited or non-existent in rural regions, where most U.S. oil and gas production operations take place (Carlton et al., 2014). Using the SCanning Imaging Absorption spectroMeter for Atmospheric CHartographY (SCIAMACHY) instrument, methane was found to be elevated in the San Juan basin, New Mexico (Kort et al., 2014). Increasing trends in NO_x were quantified over several large U.S. oil and gas production areas using tropospheric NO_2 columns from the Ozone Monitoring Instrument (OMI) (Duncan et al., 2016; Majid et al., 2017). Majid et al. (2017) derived a growth of 1-4.5% per year in NO_2 columns over large oil and gas production regions between 2010 and 2015. During this time period, production volumes in the Permian basin (TX and NM), one of the largest oil and gas production areas, rose by 17% (oil) and 8% (gas) per year. In contrast, between January 2017 and August 2019, oil and gas production volumes have more than doubled in the Permian basin, rising by about 63% (oil) and 68% (gas) per year (USEIA, 2019a). Increases on these scales raise the question to what extent the increased oil and gas industrial activities resulted in greater atmospheric emissions.

In this work, we present recent trends in NO_x emissions for select U.S. oil and natural gas production areas, using OMI satellite tropospheric NO_2 column data from January 2007 to August 2019. We show that changes in NO_2 over time can be attributed to oil and gas activity by applying a multivariate fit of activity data to the satellite NO_2 columns. For comparison, we also show NO_2 column data from the TROPOspheric Monitoring Instrument (TROPOMI).We quantify contributions of NO_x emissions that come from drilling, production and gas flaring and compare these results to the source attribution from a recently developed and expanded fuel-based NO_x emission inventory (Gorchov Negron et al., 2018).

2 Data Description and Methods

2.1 Satellite Remote Sensing Data for NO_2

OMI is a spectrometer on board NASA's EOS-Aura satellite that measures several trace gases such as NO_2, sulfur dioxide, ozone and aerosols with almost daily global coverage since 2005 (Levelt et al., 2018). For this study, we use tropospheric Vertical Column Densities (VCDs) of NO_2, which signify the total number of molecules between the

surface and the tropopause per surface area. The latest OMI NO_2 tropospheric VCD product (QA4ECV version 1.1, Boersma et al., 2018) was obtained from the Royal Dutch Meteorological Institute. To minimize bias in our multi-year trend analysis, we only use pixels from detector rows 5-25 to exclude rows with a large ground pixel size and to avoid row anomalies, a problem probably caused by an external blockage of the field of view (Schenkeveld et al., 2017). To minimize retrieval uncertainties from clouds, aerosols, snow and ice and stratospheric NO_2, the following exclusion filters were applied: cloud radiance fraction > 0.5, tropospheric and geometric AMF < 0.1, snow/ice flag > 10, surface albedo > 0.3 and solar zenith angle > 80°. VCDs from each pixel were gridded into a 0.4 by 0.4 degrees latitude/longitude grid using a surface weighted distribution, and then averaged by month. The NO_2 seasonal signal is different for each location (see e.g. van der A et al., 2008). Here we apply a seasonal correction that is based on local normalized monthly averages (see Figure S1 and Section S1 for further details).

TROPOMI is a spectrometer on board the Copernicus Sentinel-5 Precursor satellite, launched on 13 October 2017 (Veefkind et al., 2012). OMI and TROPOMI cover a comparable UV-visible wavelength range to measure NO_2. Maximum NO_2 ground pixel resolution at nadir is 3.5 x 7 km^2 for TROPOMI compared to 13 x 24 km^2 for OMI. Monthly averages were created from level 2 offline data (van Geffen et al., 2019) for May 2018 to April 2019 applying the same filters and surface grid as used for OMI data, except for using ground pixel center coordinates instead of surface weights, which creates no significant difference given the increased spatial resolution of TROPOMI. The OMI seasonal correction was applied to TROPOMI VCDs for direct comparison.

2.2. Oil and Gas Activity Data

Since 2007 the U.S. Energy Information Administration has provided monthly oil and gas activity data for key production regions in the U.S. (USEIA, 2019a). The data includes production volumes of oil in barrels per day (bbl/d) and of natural gas in thousand cubic feet per day (Mcf/d) and the number of active drill rigs. There is no distinction between oil- and gas-directed rigs because most wells produce both oil and gas. Figure 1 shows oil and gas production volumes for the Permian (TX and NM), Bakken (ND) and Eagle Ford (TX) basins. These basins are chosen as our study areas because they are among the largest oil and gas producing areas in the U.S. (USEIA, 2019a, see also Figure 2b).

Flared gas volumes are derived from the Visible Infrared Imaging Radiometer Suite (VIIRS) satellite shortwave and near-infrared data as described in Elvidge et al. (2015). Flared gas volumes for our study regions are available from March 2012 to August 2019 (Figure 1) in units of Billion Cubic Meter (BCM), with an error of +/- 0.1 BCM/year for a single flare.

2.3. Fuel-Based Oil & Gas NO_x Inventory

The Fuel-Based Oil & Gas (FOG) Inventory (Gorchov Negron et al., 2018) quantifies NO_x emissions from oil and gas production based on reported fuel records from the Energy Information Administration and NO_x emission factors reported in the literature or from the US Environmental Protection Agency's Oil and Gas Tool (USEPA, 2015). FOG uncertainties are assessed utilizing a Monte Carlo analysis. The previously published FOG inventory was for 2013. Data shown here is updated to 2015, which includes adding the Bakken basin and emissions from the New Mexico side of the Permian basin. For further details see Section S2.

3 Results and Discussion

Since January 2017, oil and gas production volumes have doubled in the Permian basin (Figure 1). Production volumes in the Bakken and Eagle Ford basins were affected by a drop in oil price in 2014/15 (Figure 1) but have since recovered. Both Permian and Bakken oil and gas production volumes are at an all-time high and, if current growth rates continue in the Eagle Ford basin, maximum production volumes will be exceeded in about one year. Figure 2a presents absolute changes in tropospheric NO_2 VCDs over the continental U.S. between 2007 and 2018. Outlines denote nine prominent U.S. oil and gas production areas. The Permian, Bakken and Eagle Ford basins show increases in NO_2. Recent increases over the Permian basin are illustrated by small insets in Figure 2a, which also show the distinction between the Delaware basin in the western half of the Permian basin and the Midland basin in the eastern half. In contrast, NO_2 has decreased over densely populated areas and urban centers, mostly because of reductions in mobile source and power plant NO_x emissions (McDonald et al., 2012; Russell et al., 2012; Tong et al., 2015). Figure 2b displays FOG NO_x emissions for the nine outlined regions, and clearly indicates that the Permian, Bakken and Eagle Ford basins have the largest NO_x emissions stemming from the oil and gas industry. Here we aim to identify the main oil and gas production sources that drive the observed changes in the NO_2 columns.

3.1 Source Attribution by Multivariate Regression to Tropospheric NO_2 VCDs

NO_x sources associated with oil and natural gas production include emissions from internal combustion engines in drill rigs, pump jacks, separators, and compressors, as well as transport vehicles and the direct combustion of natural gas in flares (Ahmadov et al., 2015; Carlton et al., 2014; Duncan et al., 2016; Kemball-Cook et al., 2010). A distinction can be drawn between drilling, production and flaring activities. During the drilling phase, heavy machinery is used to drill and hydraulically fracture a new well. Natural gas released during this process is flared. After well completion, the production phase gas begins, which requires a variety of smaller engines and transportation vehicles. Flaring of lighter hydrocarbons and natural gas occurs if their processing is not

economical (Gorchov Negron et al., 2018). All three processes vary on different time scales as indicated in Figure 1. Drilling a new well takes a few months. The number of active drill rigs responds quickly to economic changes as illustrated by the steep drop in 2015 caused by a decrease in the oil price. Production from existing wells responds more slowly to economic changes. Once a well is completed, it will continue to produce oil and natural gas for years to decades. Consequently, the large change in drilling activity in 2015 caused only small changes in production (Figure 1). Flaring varies in time somewhere in between the time scales of drilling and production.

Here we make use of the distinctly different temporal signatures of drilling, production and flaring to derive a NO_x source attribution from the observed NO_2 columns. NO_2 is used as a proxy for NO_x emissions, which inherently assumes the following: 1) NO_x is dominated by NO_2, especially when averaged over larger areas, since most NO_x is emitted as NO and then rapidly converted to NO_2. 2) The NO/NO_2 ratio has not significantly changed over time. 3) Emissions and columns are not linearly coupled but, since the lifetime of NO_x is on the order of hours it can be assumed that observed enhancements in NO_2 columns are caused by local emissions. Higher NO_2 would likely decrease the NO_2 lifetime, so that co-located NO_2 columns would be less enhanced than expected from increased emissions. However, we assume this to be a small effect, because NO_2 columns in our regions of interest are comparatively low. The same or similar assumptions were used in most previous studies (Beirle et al., 2011; Duncan et al., 2013, 2016; Laughner & Cohen, 2017; Lin et al., 2010; Liu et al., 2016; Majid et al., 2017; Nault et al., 2017).

The temporal changes in the OMI tropospheric NO_2 VCDs are attributed to specific activities by applying a multivariate regression to monthly satellite data using the oil and gas activity data shown in Figure 1 as predictors. Relative contributions for drilling, production and flaring are obtained by simultaneously fitting rig count, production volume and flared gas volume according to the following equation:

$$NO_2 = c_1 \cdot \text{background} + c_2 \cdot \text{rig count} + c_3 \cdot \text{production volume} + c_4 \cdot \text{flared gas volume} \quad (1)$$

where "NO_2" is the monthly OMI data, "background" is a constant over time and "c_1" to "c_4" are the resulting regression fit coefficients. The assumption that the background VCD is constant will be evaluated below. The standard deviation of the monthly mean NO_2 VCDs was included as error margin in the regression fits. Multivariate regression and comparable methods have been successfully applied in previous studies (He et al., 2019; Majid et al., 2017).

For this study, two sets of regression fits were performed, one fit between January 2007 and August 2019, including rig count and production volume as predictors, and a second

fit on March 2012 to April 2019 data, additionally using flared gas volume, since the latter is only available after 2012. Sensitivity to the initialization of the fit coefficients was assessed by running a series of fits that iteratively varied the initial parameters. For each fit coefficient we found a global minimum at the minimum RMS error, i.e., the difference between measured and modeled fit columns (Figure S3), which indicates convergence of the fit onto a single solution that was chosen as fit result. In the regression, data used as predictors are normalized. Oil and gas production volumes correlate strongly in time, because wells often produce both. We therefore ran each regression three times, using either oil, gas, or the normalized average of oil and gas production volumes as predictor. Differences between these three subsets were generally within error margins. The choice of production volume predictor was based on the minimum RMS error from the longer time period (2007-19) fits and was kept consistent for the shorter time period (2012-19) fits.

Figure 3a shows the regression fit results for the Permian basin. Fit coefficients, standard deviations, RMS error, and the correlation coefficient R^2 are listed in Table 1. Displayed fit coefficients are scaled by predictors to make the results directly comparable between the two time periods. Including the flared gas volume as separate predictor did not allow a statistically meaningful separation between flaring and production. Therefore, the normalized production volume and flared gas volume data were averaged and applied as one combined predictor, since they have the most similar temporal signatures (see Figure 1). The long time period fits exhibit higher R^2 values compared to the short time period fits, because the largest relative changes in in the NO_2 columns are before 2012, which gives a better constraint on the fits. Results for the same analysis for the Bakken and Eagle Ford regions are displayed in Figures S4a and S5a. Tables S1-S3 give a summary of all regression results.

Figures 3b, S4b and S5b show the derived NO_2 partial VCDs expressed as fractions attributed to drilling versus production (from the 2007-2019 fits) and drilling versus combined production+flaring (from the 2012-2019 fits). In the first part of the record, emissions were dominated by drilling in all three basins, but in recent years the production itself has become responsible for a larger fraction of emissions, possibly because the industry became more efficient and produced a larger volume of oil per well (UAEIA, 2019a). These findings are robust between both sets of regression fits. For example, the scaled fit coefficient for drilling is the same for the two different multivariate regressions presented in Table 1.

In order to compare source attributions between the three basins, the NO_2 column enhancement per drill rig and per production volume are calculated for each region (Figure S6). These parameters can be compared between basins assuming that effects from differences in meteorology and NO_x lifetimes are smaller than our error bars. For

most fit parameters we find agreement across regions within error margins, which strengthens the plausibility of the regression results.

The NO_2 partial VCD contributions attributed to oil and gas are relatively small compared to both the magnitude of the fitted background and the OMI NO_2 data variability. We therefore conducted sensitivity studies on the effect of our constant background correction, data variability, and seasonal correction.

Background correction: In our regressions, the NO_2 background is a constant, which is based on the following assumptions: 1) NO_x emissions from oil and gas are the dominant NO_x source in our study areas; 2) the background in these rather remote areas is much less affected by the strong NO_x trends seen in metropolitan regions; and 3) other NO_x sources change on temporal scales that are either averaged out by the monthly means or are sufficiently small to be contained in the error margins of our fit results. To validate these assumptions, we looked at trends in VCDs from a neighboring region without oil and gas production (see Figure S7). For all three study areas, these backgrounds show no significant trend over time and compare within error margins to the background fit coefficients from the regressions. This indicates that temporal changes over time within the study areas are dominated by oil and gas NO_x emissions. Further details are described in Section S3.

Data variability and seasonal correction: To investigate the effect of data noise and seasonal correction, we ran the long time period regression fits on annually averaged NO_2 VCDs fits using annually averaged oil and gas industry activity data. Annual means inherently average out the seasonal signal and strongly reduce data variability. Despite the reduced information content of the annual data set, most fit coefficients (Table S4) agree within error margins with the monthly results, but with much higher R^2 values of, e.g., 0.653 versus 0.397 for the Permian basin (Tables 1 and S1-S3). This outcome indicates that neither the data variability nor an incomplete seasonal correction of the NO_2 monthly averages poses a fundamental limitation to our analysis. (For further discussion, see Section S4.)

Since 2017, the TROPOMI instrument has obtained global tropospheric NO_2 columns on a daily basis. We included TROPOMI NO_2 VCDs in Figures 3a, S4a and S5a. We find overall good agreement, with a mean difference of -4%, +14%, and -14% for the Permian, Bakken and Eagle Ford basins, respectively (see Section S5 for further discussion). The variability in the TROPOMI data is smaller. The agreement between OMI and TROPOMI VCDs is encouraging for future long-term trend studies on a combined data set. For comparison, Figure S9 shows a map of OMI and TROPOMI tropospheric NO_2 VCDs over the Permian basin for August 2018.

3.2. Comparison with Source Attribution from FOG

FOG NO_x source attribution data is available for 2013 for the Permian basin and for 2015 for both, the Permian and Bakken basins. The NO_2 source attributions derived from the multivariate regressions are compared with the FOG inventory in Figures 3b and S4b. We have added flaring emissions to FOG using annual averages of the flared gas volumes to calculate NO_x emissions based on best estimates for the heat content of natural gas and a conversion factor that correlates heating value with NO_x emissions (Torres et al., 2012, USEIA, 2019d; see Section S6 for further details). A comparison of NO_x emissions coming from drilling and production (FOG) and from flaring is shown in Figure S10. The agreement between the regression results and FOG data is excellent and well within error margins. FOG and satellite data agree within 3 (2013) and 4 (2015) percentage points for the Permian basin and within 8 percentage points for the Bakken basin. The Permian comparison also shows that trends over time are captured by both methods. Based on our NO_x emissions estimates, the fraction for flaring in 2015 is 7± 0.3% and 11±1% for the Permian and Bakken basins, corresponding to 8.7±0.5 and 7.5±0.5 tons of NO_x per day. Flaring estimates for 2018 are 12.6±0.6 and 11±0.6 tons of NO_x per day for the Permian and Bakken basins, respectively. If recent trends in production and flaring continue, a significant separation of drilling, production and flaring might be possible using OMI satellite data and seems feasible using TROPOMI data.

4 Conclusions

Recent trends in U.S. oil and gas production have led to increased emissions of NO_x that are captured by satellite measurements of tropospheric NO_2 columns. Oil and gas activity data were successfully used as predictors in a multivariate regression to explain observed changes in the NO_2 VCDs over time as a combination of drilling, production and flaring activities. Comparison with the FOG NO_x emission inventory shows good agreement between top-down and bottom-up source attributions for the Permian and Bakken regions. We conclude that satellite measurements of tropospheric NO_2 are a good proxy to track oil and gas NOx emissions and retrieve source attributions, as long as NO_x emissions from oil and gas are a large NO_x source in the region.

Acknowledgments, and Data

The following data used in this study are publicly available:

OMI NO_2 data (Boersma, 2017) and TROPOMI NO_2 data (http://doi.org/10.5270/S5P-s4ljg54**)**. We acknowledge the free use of tropospheric NO_2 column data from the OMI sensor from www.temis.nl. This work uses modified OMI VCDs for 2007 to 2019 and modified Copernicus Sentinel data for 2018 and 2019.

Annual flared gas volumes at www.ngdc.noaa.gov/eog/viirs/download_global_flare.html

We acknowledge helpful discussions with Ronald van der A and Henk Eskes, and support from Bud Pope. This work was financially supported by the NASA ACMAP program under award number 80NSSC19K0979, by the Colorado Energy Research Collaboratory under project number #31-2018, and by the NOAA cooperative institute agreement under award number NA17OAR4320101.

References

van der A, R. J., Eskes, H. J., Boersma, K. F., van Noije, T. P. C., Van Roozendael, M., De Smedt, I., et al. (2008). Trends, seasonal variability and dominant NO_x source derived from a ten year record of NO_2 measured from space. *Journal of Geophysical Research*, *113*(D4), D04302. https://doi.org/10.1029/2007JD009021

Ahmadov, R., McKeen, S., Trainer, M., Banta, R., Brewer, A., Brown, S., et al. (2015). Understanding high wintertime ozone pollution events in an oil- and natural gas-producing region of the western US. *Atmospheric Chemistry and Physics*, *15*(1), 411–429. https://doi.org/10.5194/acp-15-411-2015

Alvarez, R. A., Pacala, S. W., Winebrake, J. J., Chameides, W. L., & Hamburg, S. P. (2012). Greater focus needed on methane leakage from natural gas infrastructure. *Proceedings of the National Academy of Sciences*, *109*(17), 6435–6440. https://doi.org/10.1073/pnas.1202407109

Alvarez, Ramón A., Zavala-Araiza, D., Lyon, D. R., Allen, D. T., Barkley, Z. R., Brandt, A. R., et al. (2018). Assessment of methane emissions from the U.S. oil and gas supply chain. *Science*, *361*(6398), 186–188. https://doi.org/10.1126/science.aar7204

Beirle, S., Boersma, K. F., Platt, U., Lawrence, M. G., & Wagner, T. (2011). Megacity emissions and lifetimes of mitrogen oxides probed from space. *Science*, *333*(6050), 1737–1739. https://doi.org/10.1126/science.1207824

Boersma, K. F., Eskes, H., Richter, A., De Smedt, I., Lorente, A., Beirle, S., Van Geffen, J., Peters, E., Van Roozendael, M., & Wagner, T. (2017). QA4ECV NO_2 tropospheric and stratospheric vertical column data from OMI (Version 1.1) [Data set]. Royal Netherlands Meteorological Institute (KNMI). http://doi.org/10.21944/qa4ecv-no2-omi-v1.1

Boersma, K. F., Eskes, H. J., Richter, A., De Smedt, I., Lorente, A., Beirle, S., et al. (2018). Improving algorithms and uncertainty estimates for satellite NO_2 retrievals: results from the quality assurance for the essential climate variables (QA4ECV) project. *Atmospheric Measurement Techniques*, *11*(12), 6651–6678. https://doi.org/10.5194/amt-11-6651-2018

Brandt, A. R., Heath, G. A., Kort, E. A., O'Sullivan, F., Petron, G., Jordaan, S. M., et al. (2014). Methane leaks from North American natural gas systems. *Science*, *343*(6172), 733–735. https://doi.org/10.1126/science.1247045

Carlton, A. G., Little, E., Moeller, M., Odoyo, S., & Shepson, P. B. (2014). The data gap: Can a lack of monitors obscure loss of clean air act benefits in fracking areas? *Environmental Science & Technology*, *48*(2), 893–894. https://doi.org/10.1021/es405672t

Duncan, B. N., Yoshida, Y., de Foy, B., Lamsal, L. N., Streets, D. G., Lu, Z., et al. (2013). The observed response of Ozone Monitoring Instrument (OMI) NO_2 columns to NO_x emission controls on power plants in the United States: 2005–2011. *Atmospheric Environment*, *81*, 102–111. https://doi.org/10.1016/j.atmosenv.2013.08.068

Duncan, B. N., Lamsal, L. N., Thompson, A. M., Yoshida, Y., Lu, Z., Streets, D. G., et al. (2016). A space-based, high-resolution view of notable changes in urban NO_x pollution around the world (2005-2014). *Journal of Geophysical Research: Atmospheres*, *121*(2), 976–996. https://doi.org/10.1002/2015JD024121

Edwards, P. M., Brown, S. S., Roberts, J. M., Ahmadov, R., Banta, R. M., deGouw, J. A., et al. (2014). High winter ozone pollution from carbonyl photolysis in an oil and gas basin. *Nature*, *514*(7522), 351–354. https://doi.org/10.1038/nature13767

Elvidge, C., Zhizhin, M., Baugh, K., Hsu, F.-C., & Ghosh, T. (2015). Methods for global survey of natural gas flaring from Visible Infrared Imaging Radiometer Suite data. *Energies*, *9*(1),

14. https://doi.org/10.3390/en9010014

Gorchov Negron, A. M., McDonald, B. C., McKeen, S. A., Peischl, J., Ahmadov, R., de Gouw, J. A., et al. (2018). Development of a Fuel-Based Oil and Gas Inventory of Nitrogen Oxides Emissions. *Environmental Science & Technology*, *52*(17), 10175–10185. https://doi.org/10.1021/acs.est.8b02245

de Gouw, J. A., Parrish, D. D., Frost, G. J., & Trainer, M. (2014). Reduced emissions of CO_2, NO_x, and SO_2 from U.S. power plants owing to switch from coal to natural gas with combined cycle technology. *Earth's Future*, *2*(2), 75–82. https://doi.org/10.1002/2013EF000196

He, L., Zeng, Z., Pongetti, T. J., Wong, C., Liang, J., Gurney, K. R., et al. (2019). Atmospheric methane emissions correlate with natural gas consumption from residential and commercial sectors in Los Angeles. *Geophysical Research Letters*, *46*(14), 8563–8571. https://doi.org/10.1029/2019GL083400

Howarth, R. W., Ingraffea, A., & Engelder, T. (2011). Should fracking stop? *Nature*, *477*(7364), 271–275. https://doi.org/10.1038/477271a

Karion, A., Sweeney, C., Pétron, G., Frost, G., Hardesty, R. M., Kofler, J., et al. (2013). Methane emissions estimate from airborne measurements over a western United States natural gas field. *Geophysical Research Letters*, *40*(16), 4393–4397. https://doi.org/10.1002/grl.50811

Kemball-Cook, S., Bar-Ilan, A., Grant, J., Parker, L., Jung, J., Santamaria, W., et al. (2010). Ozone impacts of natural gas development in the Haynesville Shale. *Environmental Science & Technology*, *44*(24), 9357–9363. https://doi.org/10.1021/es1021137

Kort, E. A., Frankenberg, C., Costigan, K. R., Lindenmaier, R., Dubey, M. K., & Wunch, D. (2014). Four corners: The largest U.S. methane anomaly viewed from space. *Geophysical Research Letters*, *41*(19), 6898–6903. https://doi.org/10.1002/2014GL061503

Laughner, J. L., & Cohen, R. C. (2017). Quantification of the effect of modeled lightning NO_2 on UV–visible air mass factors. *Atmospheric Measurement Techniques*, *10*(11), 4403–4419. https://doi.org/10.5194/amt-10-4403-2017

Levelt, P. F., Joiner, J., Tamminen, J., Veefkind, J. P., Bhartia, P. K., Stein Zweers, D. C., et al. (2018). The Ozone Monitoring Instrument: overview of 14 years in space. *Atmospheric Chemistry and Physics*, *18*(8), 5699–5745. https://doi.org/10.5194/acp-18-5699-2018

Lin, J.-T., McElroy, M. B., & Boersma, K. F. (2010). Constraint of anthropogenic NO_x emissions in China from different sectors: a new methodology using multiple satellite

retrievals. *Atmospheric Chemistry and Physics*, *10*(1), 63–78. https://doi.org/10.5194/acp-10-63-2010

Liu, F., Beirle, S., Zhang, Q., Dörner, S., He, K., & Wagner, T. (2016). NO_x lifetimes and emissions of cities and power plants in polluted background estimated by satellite observations. *Atmospheric Chemistry and Physics*, *16*(8), 5283–5298. https://doi.org/10.5194/acp-16-5283-2016

Majid, A., Val Martin, M., Lamsal, L. N., & Duncan, B. N. (2017). A decade of changes in nitrogen oxides over regions of oil and natural gas activity in the United States. *Elementa: Science of the Anthropocene*, *5*(0), 76. https://doi.org/10.1525/elementa.259

McDonald, B. C., Dallmann, T. R., Martin, E. W., & Harley, R. A. (2012). Long-term trends in nitrogen oxide emissions from motor vehicles at national, state, and air basin scales. *Journal of Geophysical Research: Atmospheres*, *117*(D21), D00V18. https://doi.org/10.1029/2012JD018304

Nault, B. A., Laughner, J. L., Wooldridge, P. J., Crounse, J. D., Dibb, J., Diskin, G., et al. (2017). Lightning NO_x emissions: Reconciling measured and modeled estimates with updated NO_x chemistry. *Geophysical Research Letters*, *44*(18), 9479–9488. https://doi.org/10.1002/2017GL074436

Russell, A. R., Valin, L. C., & Cohen, R. C. (2012). Trends in OMI NO_2 observations over the United States: effects of emission control technology and the economic recession. *Atmospheric Chemistry and Physics*, *12*(24), 12197–12209. https://doi.org/10.5194/acp-12-12197-2012

Schenkeveld, V. M. E., Jaross, G., Marchenko, S., Haffner, D., Kleipool, Q. L., Rozemeijer, N. C., et al. (2017). In-flight performance of the Ozone Monitoring Instrument. *Atmospheric Measurement Techniques*, *10*(5), 1957–1986. https://doi.org/10.5194/amt-10-1957-2017

Tong, D. Q., Lamsal, L., Pan, L., Ding, C., Kim, H., Lee, P., et al. (2015). Long-term NO_x trends over large cities in the United States during the great recession: Comparison of satellite retrievals, ground observations, and emission inventories. *Atmospheric Environment*, *107*, 70–84. https://doi.org/10.1016/j.atmosenv.2015.01.035

Torres, V. M., Herndon, S., Wood, E., Al-Fadhli, F. M., & Allen, D. T. (2012). Emissions of nitrogen oxides from flares operating at low flow conditions. *Industrial & Engineering Chemistry Research*, *51*(39), 12600–12605. https://doi.org/10.1021/ie300179x

U.S. Energy Information Administration (2019a). Drilling Productivity Report. Retrieved from www.eia.gov/petroleum/drilling/

U.S. Energy Information Administration (2019b). Petroleum & other Liquids. Spot prices. Retrieved from www.eia.gov/dnav/pet/pet_pri_spt_s1_d.htm

U.S. Energy Information Administration (2019c). Natural Gas, Natural Gas Prices. Retrieved from/www.eia.gov/dnav/ng/ng_pri_sum_dcu_nus_m.htm

U.S. Energy Information Administration (2019d). Natural Gas, Heat Content of Natural Gas Consumed. Retrieved from www.eia.gov/dnav/ng/ng_cons_heat_a_EPG0_VGTH_btucf_a.htm

U.S. Environmental Protection Agency (2015). EPA Nonpoint Oil and Gas Emission Estimation Tool for the 2014 NEI.

Van Geffen, J. H. G. M., Eskes, H. J., Boersma, K. F., Maasakkers, J. D., Veefkind, J. P. (2019). TROPOMI ATBD of the Total and Tropospheric NO_2. *Data Products*.

Veefkind, J. P., Aben, I., McMullan, K., Förster, H., de Vries, J., Otter, G., et al. (2012). TROPOMI on the ESA Sentinel-5 Precursor: A GMES mission for global observations of the atmospheric composition for climate, air quality and ozone layer applications. *Remote Sensing of Environment, 120*, 70–83. https://doi.org/10.1016/j.rse.2011.09.027

World Health Organization (2005). Air quality guidelines, global update 2005: particulate matter, ozone, nitrogen dioxide and sulfur dioxide.

Predictor	Scaled Fit Coefficient $x10^{14}$	RMS error $x10^{14}$ [molec/cm^2]	R^2 monthly	R^2 annually
Permian basin 2007-2019				
Background	9.7 ± 0.2			
Prod. Volume (oil)	0.7 ± 0.4	1.702	0.397	0.653
Rig Count	3.3 ± 0.7			
Permian basin 2012-2019				
Background	9.6 ± 0.3			
Prod. Volume (oil) + Flared Gas Volume	0.7 ± 0.3	1.727	0.236	0.520
Rig Count	3.3 ± 0.6			

Table 1. Multivariate regression fit results for the Permian basin. Fit coefficients are scaled by predictor values from January 2014 and denote NO_2 column for the background, NO_2 column per production and flared gas volume, and per drill rigs.

Figure 1. Oil and gas activity data for the Permian, Bakken and Eagle Ford basins. The panels on top display time series of the oil (USEIA, 2019b) and gas price (United States natural gas industrial price, USEIA 2019c).

Figure 2. OMI NO_2 map and FOG NO_x emission estimates. (a) Absolute changes in OMI tropospheric NO_2 VCDs between 2007 and 2018 for the continental U.S. Green boxes denote major U.S. oil and gas production regions. The insets show the NO_2 VCD change between 2007 and 2016, 2017 and 2018, respectively, over the Permian basin. (b) 2015 FOG NO_x emission estimates for the areas outlined in (a).

Figure 3. Multivariate regression results and fractional source attributions for the Permian basin. (a) Measured OMI tropospheric NO_2 column time series and the modelled NO_2 time series separated by multivariate fitting into a constant background column and partial NO_2 columns for drilling, production and combined production+flaring activities. (b) Comparison of fractional contributions retrieved from NO_2 partial columns and the FOG inventory.

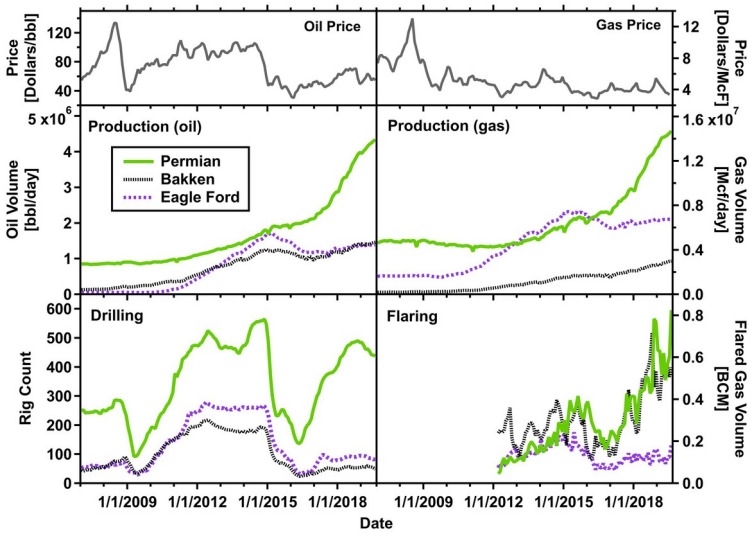

2019GL085866-f01-z-.jpg

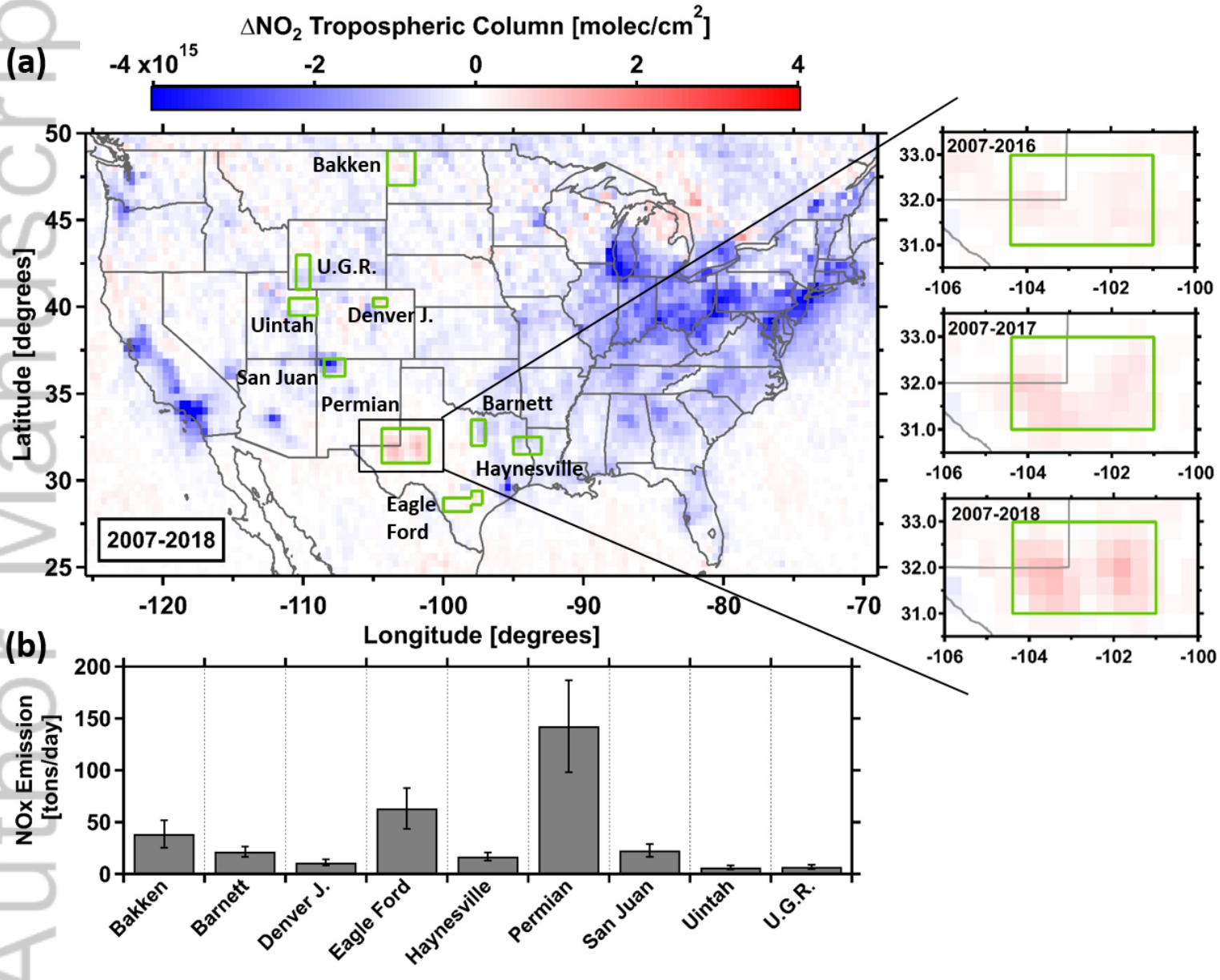

2019GL085866-f02-z-.png

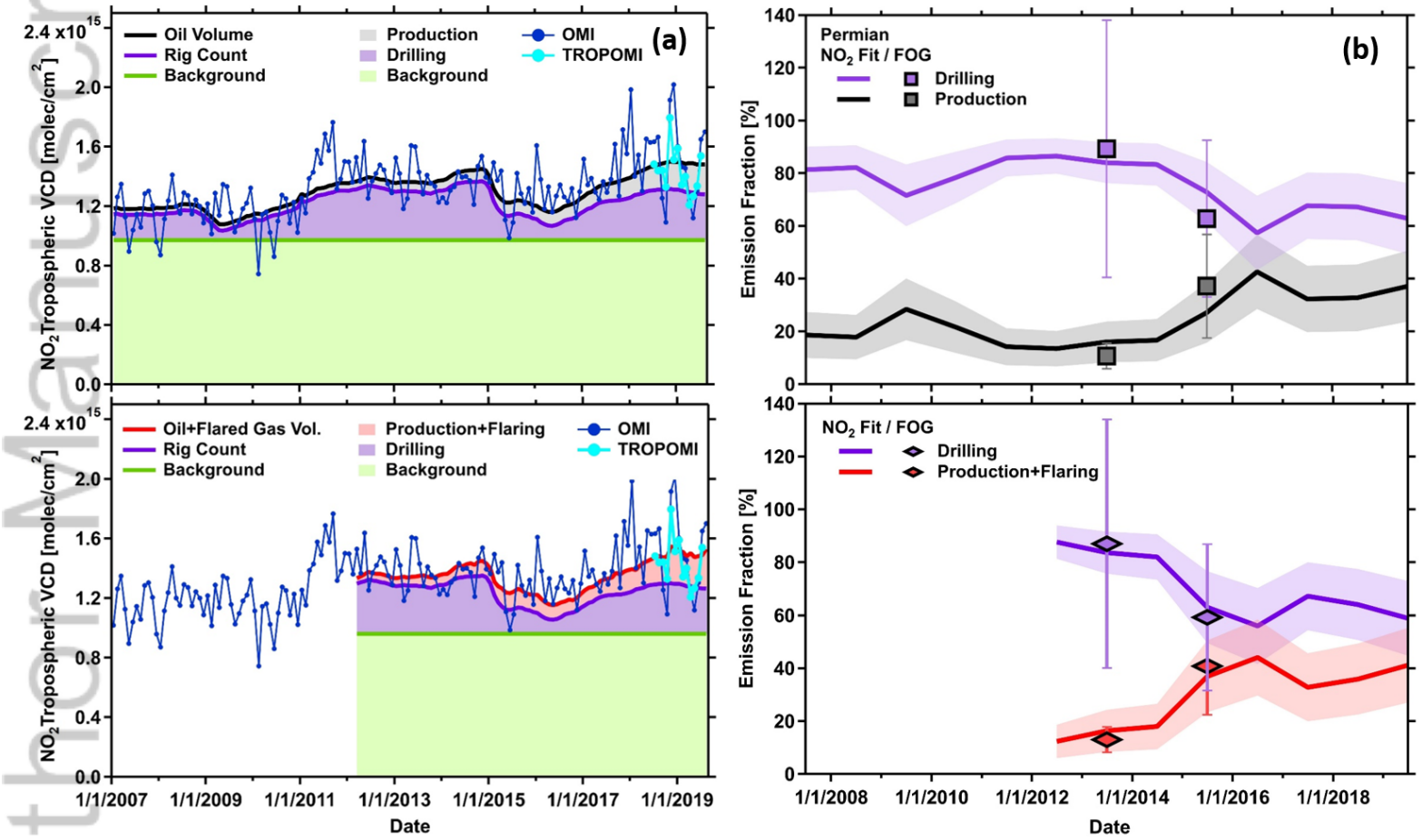

2019GL085866-f03-z-.png